Pharm Res (2013) 30:2832–2842
DOI 10.1007/s11095-013-1111-7

RESEARCH PAPER

Mitochondrial Delivery of Doxorubicin by Triphenylphosphonium-Functionalized Hyperbranched Nanocarriers Results in Rapid and Severe Cytotoxicity

Theodossis A. Theodossiou • Zili Sideratou • Maria E. Katsarou • Dimitris Tsiourvas

Received: 22 March 2013 / Accepted: 4 June 2013 / Published online: 7 August 2013

ABSTRACT

Purpose To develop a novel hyperbranched polymer-based nanocarrier for efficient drug delivery to cell mitochondria. Also to study for the first time the cytotoxic effect of doxorubicin *via* mitochondria-specific delivery system.

Methods We introduced alkyltriphenylphosphonium groups (TPP) to a poly(ethylene imine) hyperbranched polymer (PEI). We harnessed the hydrophobic assembly of these alkylTPP functionalized PEI molecules into ~100 nm diameter nanoparticles (PEI-TPP) and further encapsulated the chemotherapy agent doxorubicin (DOX), to produce the mitotropic nanoparticles PEI-TPP-DOX.

Results By administering PEI-TPP-DOX to human prostate carcinoma cells DU145, we found that: (i) PEI-TPP-DOX specifically localized at cell mitochondria as revealed by the inherent DOX fluorescence; (ii) in contrast to the slow apoptotic cell death incurred by DOX over the period of days at micromolar concentrations, PEI-TPP-DOX triggered rapid and severe cytotoxicity within few hours of incubation and at submicromolar incubation concentrations. This cytotoxicity was mainly found to be of a necrotic nature, not precluding autophagy related death pathways to a smaller extent.

Conclusions We have elaborated a versatile mitotropic nanocarrier; furthermore, using this platform, we have developed a mitochondrial-doxorubicin formulation with exceptional cytocidal properties, even in nanomolar concentrations.

KEY WORDS cytotoxicity · doxorubicin · hyperbranched poly(ethylene imine) · mitochondrial drug delivery · triphenylphosphonium

ABBREVIATIONS

ANT	Adenine nucleotide translocator
ANTI-A	Antimycin A
ATR	Atractyloside potassium salt
CASP8	Z-IETD-FMK
CASP9	Z-LEHD-FMK
CCCP	Carbonyl cyanide 3-chlorophenylhydrazone
CSA	Cyclosporine A
DIPEA	*N,N*-diisopropylethylamine
DLS	Dynamic light scattering
DOX	Doxorubicin
EB	Ethidium bromide
EPR	Enhanced permeability and retention
ETC	Electron transport chain
FBS	Fetal bovine serum
HBTU	2-(1H-benzotriazole-1-yl)-1,1,3,3-tetramethyluronium
HOBt	*N*-hydroxybenzotriazole
LDH	Lactate dehydrogenase
L-NAME	*Nω*-nitro-L-arginine methyl ester hydrochloride
MnTmPyP	Mn(III)tetrakis(1-methyl-4-pyridyl)porphyrin
MPTP	Mitochondrial permeability transition pore
MTT	Thiazolyl blue tetrazolium bromide
MYXO	Myxothiazol
NADH	β-Nicotinamide adenine dinucleotide reduced disodium salt
OLIGO	Oligomycin
PBS	Phosphate buffer saline
PEI	Hyperbranched poly(ethylene imine)
PNNAG	*p*-nitrophenyl-*N*-acetyl-β-D-glucosaminide
ROS	Reactive oxygen species
ROT	Rotenone
RUR	Ruthenium red

Electronic supplementary material The online version of this article (doi:10.1007/s11095-013-1111-7) contains supplementary material, which is available to authorized users.

T. A. Theodossiou (✉) · Z. Sideratou · M. E. Katsarou · D. Tsiourvas
Department of Physical Chemistry, IAMPPNM
NCSR "Demokritos", Patriarchou Gregoriou & Neapoleos
15310 Ag. Paraskevi, Attiki, Greece
e-mail: theo@chem.demokritos.gr

T. A. Theodossiou
e-mail: t.theodossiou@gmail.com

STS	Staurosporine
TB	Trypan blue
TPP	Triphenylphosphonium cation
TTFA	Thenoyltrifluoroacetone
UA	Uric acid
WORT	Wortmannin

INTRODUCTION

Mitochondria are the "power stations" of eukaryotic cells where energy derived from the oxidation of reducing substrates is converted through the shuttling of electrons along inner membrane electron transport chain (ETC) to ATP *via* oxidative phosphorylation (1), using oxygen as a terminal electron acceptor; ATP is subsequently distributed intracellularly to manage the energy requirements of all vital functions. In non-inflammatory cells, mitochondria are also the main source of intracellular reactive oxygen species (ROS) and therefore are major mediators of important ROS signalling in cells (2,3).

More recently, the importance of mitochondria in controlling the response to cell death signals has been established (4). Mitochondria are crucial checkpoints for the *intrinsic* (or mitochondrial) pathway of apoptosis; nevertheless, mitochondria are also involved in autophagic cell death (mitophagy) and necrotic cell demise following direct, irreversible mitochondrial damage.

The need for specific delivery of therapeutic agents or mitochondrial DNA (mtDNA) to cell mitochondria has recently constituted a hot research focus. This can be attributed to the progressive identification of mitochondrial dysfunctions and mtDNA mutations as the underlying causes of several and diverse pathologies (5–8).

Drug delivery to cell mitochondria (9,10) can be achieved *via* direct chemical conjugation of the selected bioactive molecules with mitotropic ligands. In this context, cell/mitochondria penetrating peptides (11–14), the lipophilic alkylated triphenylphosphonium cation (TPP) (8,15–20) and the guanidinium group (21,22) have successfully been applied to target their conjugated cargo-compounds to mitochondria. This bespoke synthetic approach is however applicable to one therapeutic agent at a time and also restricted by the caveat that the chemically conjugated agents retain their original, free-drug therapeutic activity. Alternative strategies employing the use of Trojan-horse nanocarriers functionalized with the appropriate targeting ligands are becoming increasingly popular as they can constitute generic platforms for loading a diversity of therapeutic agents and could also be potentially useful for mtDNA transduction. The implementation of such *mitotropic* vehicles is intensively pursued (23–34), within the forefront research area of subcellular organelle targeted drug delivery (35–37). Mitotropic nanocarrier implementation has so far mainly focused on the development *of mitochondriotropic liposomes* (31,33,35,38–41) through introduction of appropriate ligands on the liposomal surfaces which were subsequently loaded with selected drugs either in their aqueous cores or lipid bilayers.

Recently, however, this research started to encompass the development of dendrimeric mitotropic carriers (30,32,34,42,43). In a recent work (34) we presented the development of a mitotropic nanocarrier based on an oligolysine scaffold *via* addition of two alkylated TPP cations per oligomer. The TPP modified carrier demonstrated striking mitochondrial specificity with or without the attachment of a cargo molecule, D-Luciferin, which exhibited long steady-state chemiluminescence.

Herein, we introduced the lipophilic decylTPP group to a poly(ethylene imine) hyperbranched polymer having an average molecular weight of 1300 (PEI) through an amide bond formation. The resulting compound, being water insoluble, had the tendency to form sub-μm particles in water. We were further able to control the hydrophobic assembly of TPP functionalized PEI molecules into ~100 nm mean diameter nanoparticles (PEI-TPP) and proceeded with the encapsulation of doxorubicin (DOX), a natural anthracycline glycoside and topoisomerase II inhibitor (44), to produce the mitotropic nanocarriers, PEI-TPP-DOX.

MATERIALS AND METHODS

Chemicals and Reagents

RPMI 1640 and OPTIMEM without phenol red, fetal bovine serum (FBS), penicillin/streptomycin, L-glutamine, phosphate buffer saline (PBS), MitoTracker® Green FM and trypsin/versene were all purchased from Invitrogen Ltd. (Paisley,UK). Low melting point agarose was obtained from GENAXYS. Thiazolyl blue tetrazolium bromide (MTT), dimethyl sulfoxide (DMSO), antimycin A (ANTI-A), oligomycin (OLIGO), myxothiazol (MYXO), sodium azide (NaN_3), rotenone (ROT), thenoyltrifluoroacetone (TTFA), carbonyl cyanide 3-chlorophenylhydrazone (CCCP), atractyloside potassium salt (ATR), *Nω*-nitro-L-arginine methyl ester hydrochloride (L-NAME), uric acid (UA), ruthenium red (RUR), β-Nicotinamide adenine dinucleotide, reduced disodium salt (NADH), *p*-nitrophenyl-*N*-acetyl-β-D-glucosaminide (PNNAG), citrate, glycine, ethylenediaminetetraacetic acid (EDTA), trizma® hydrochloride (Tris–HCl), sodium pyruvate, triton-X-100, staurosporine (STS), ethidium bromide (EB), SDS, proteinase K, ribonuclease A, *N,N*-diisopropylethylamine (DIPEA) and triphenylphosphine, were purchased from Sigma-Aldrich Ltd. (Poole, UK). Z-IETD-FMK (caspase 8 inhibitor, CASP8) and Z-LEHD-FMK (caspase 9 inhibitor, CASP9) were obtained from R&D Systems Europe Ltd (Abingdon, UK). BAPTA-AM, Mn(III)tetrakis(1-methyl-4-pyridyl)porphyrin (MnTmPyP), wortmannin (WORT) and

cyclosporine A (CSA) were purchased from Merck KGaA (Calbiochem®, Darmstadt, Germany). *N*-hydroxybenzotriazole (HOBt) and 2-(1H-benzotriazole-1-yl)-1,1,3,3-tetramethyluronium (HBTU) were purchased from Anaspec (San Jose, USA). Finally, doxorubicin hydrochloride (DOX) and branched poly(ethylene imine) (PEI) with a molecular weight of 1300 Da (Lupasol® G20, water-free, 98%) were kindly donated by Regulon SA (Athens, Greece) and BASF (Ludwigshafen, Germany), respectively.

Synthesis of PEI-TPP

The introduction of alkylTPP groups to PEI was realized in two steps. In the first step, (10-carboxydecyl)triphenylphosphonium bromide was synthesized according to a recently reported procedure described in our previous paper (34), while in the second step this derivative was reacted with the primary amino groups of PEI, affording PEI-TPP (Scheme 1). Briefly, 1 mmol of (10-carboxydecyl)triphenylphosphonium bromide, dissolved in 10 mL of anhydrous DMF was added to 0.4 mmol of PEI, dissolved in 10 mL of dry DMF. Subsequently, HBTU (1.6 mmol) and HOBt (1.6 mmol) dissolved in 2 mL DMF were added to the mixture, followed by addition of DIPEA (1.6 mmol). The mixture was allowed to react overnight, under argon atmosphere, at room temperature. The solvent was partially removed under vacuum and the product was twice precipitated with diethyl ether (75% yield). The structure of PEI-TPP was established by proton and carbon NMR spectroscopy using a Bruker Avance DRX spectrometer operating at 500 and 125.1 MHz, respectively. The degree of substitution was determined by inverse-gated decoupling ^{13}C NMR.

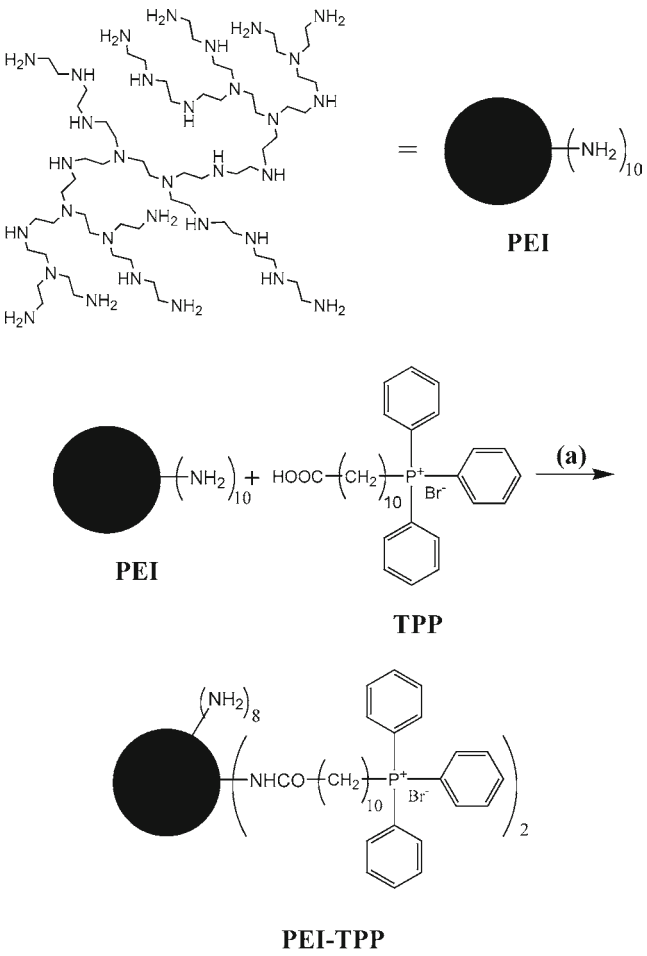

Scheme 1 Synthesis of PEI-TPP: (*a*) PEI (0.4 mmol), (10-carboxydecyl) triphenylphosphonium bromide (1 mmol), HBTU (1.6 mmol), HOBt (1.6- mmol), DIPEA (1.6 mmol), dry DMF, overnight, argon atmosphere, room temperature, 75% yield.

^{1}H NMR (500 MHz, MeOD-d_4): δ = 1.12–1.40 (m, aliphatic CH_2), 1.40–1.70 (m, $C\underline{H}_2CH_2P^+Ph_3$, $NHCOCH_2C\underline{H}_2$), 2.06–2.20 (t, $NHCOC\underline{H}_2$), 2.45–2.85 (m, CH_2 of PEI skeleton), 2.90–3.05 ($C\underline{H}_2NHCO$), 3.3–3.45 (m, $C\underline{H}_2P^+Ph_3$), 7.60–7.80 (m, aromatic H).

^{13}C NMR (125.1 MHz, MeOD-d_4): δ = 175.1 (C=O), 135.9 (P^+Ph_3 para), 133.4 (d, $\mathcal{J}$ = 10.3 Hz, P^+Ph_3 ortho/meta), 130.2 (d, $\mathcal{J}$ = 13.47 Hz, P^+Ph_3 ortho/meta), 123.7 (d, $\mathcal{J}$ = 11.67 Hz, P^+Ph_3 ipso), 55–49 ($N\underline{C}H_2\underline{C}H_2N$), 36.7–40.6 ($NH_2\underline{C}H_2$, $\underline{C}H_2NHCO$), 35.7 ($CONH\underline{C}H_2$), 30.4 (d, $\mathcal{J}$ = 17.17 Hz, $\underline{C}H_2CH_2CH_2P^+Ph_3$), 29.5–28.2 (aliphatic $\underline{C}H_2$), 22.1 ($CH_2P^+Ph_3$), 21.4 (d, $\mathcal{J}$ = 31.50 Hz, $\underline{C}H_2CH_2P^+Ph_3$).

Preparation and Characterization of PEI-TPP and PEI-TPP-DOX Nanoparticles

PEI-TPP nanoparticles as well as DOX loaded PEI-TPP nanoparticles were prepared by the dropwise addition, of a DMSO PEI-TPP solution to OPTIMEM or to a DOX OPTIMEM solution respectively, under rigorous stirring. Specifically, a 34 mM PEI-TPP solution in DMSO was prepared and used as stock. For unloaded nanoparticles, 200 μL of PEI-TPP stock solution were added drop-wise to 4 ml OPTIMEM under vigorous stirring. Nanoparticles were spontaneously formed and subjected to further characterization. To prepare DOX-loaded nanoparticles, a 2 mM DOX solution in OPTIMEM was used instead of plain OPTIMEM. In order to remove non-encapsulated DOX, the obtained nanoparticles were in all cases centrifuged at 95,000 rpm for 45 min employing an OptimaTM Max Ultracentrifuge Beckman Coulter, Inc. coupled with TLN-120 rotor. The resulting pellets were washed and centrifuged as above, for a further three times with OPTIMEM to ensure complete removal of non-encapsulated DOX. The pellets were finally resuspended in 1 mL of OPTIMEM and the suspension was ultrasonicated using an ultrasonic processor UP200S, (Heilscher-Ultrasound Technology) to finely disperse the nanoparticles. The resulting dispersions were syringe-filtered through sterile nylon membrane filters of 0.20 μm pore size.

Determination of DOX

For the determination of DOX encapsulated in PEI-TPP nanocarriers, a calibration curve for various DOX concentrations (10–100 μM) in DMSO also containing 40 μM PEI-TPP was constructed using a Cary 100 Conc UV-Visible spectrophotometer (Varian Inc.) by registering absorbances at 561 nm. For every batch prepared, PEI-TPP-DOX nanoparticle dispersion aliquots (50 μL) were diluted in 700 μL of DMSO to ensure complete nanoparticle dissolution. The absorbance at 561 nm was each time registered using the same experimental conditions as those applied for the calibration curve construction, and DOX concentrations were calculated.

The size distributions of PEI-TPP and PEI-TPP-DOX nanoparticles were determined by Dynamic light scattering (DLS) employing an AXIOS-150/EX (Triton Hellas) apparatus with a 30 mW laser source, and an Avalanche photodiode detector at a 90° angle. For these experiments, 200 μL dispersions of PEI-TPP or PEI-TPP-DOX nanoparticles were used. At least ten light scattering measurements were collected for each dispersion and the results were averaged. ζ-potential measurements were conducted using ZetaPlus (Brookhaven Instruments Corp, USA). In a typical experiment, 200 μL dispersions of PEI-TPP or PEI-TPP-DOX nanoparticles were diluted into 1.4 mL water. For each dispersion, ten ζ-potential measurements were collected and the results were averaged.

Cell Culture

Cells used in this study were the human prostate carcinoma cell line DU145. The cells were grown in RPMI 1640 without phenol red, with 10% FBS, penicillin/streptomycin at 37°C in a 5% CO2 humidified atmosphere. Cell incubation with PEI-TPP or PEI-TPP-DOX (and consequently with DOX) was always performed in OPTIMEM (without phenol red).

Fluorescence Microscopy in Cells

DU145 cells were inoculated on 22 mm cover slips housed in 35 mm petri dishes (10×10^5) and left to grow overnight in 2 ml of complete RPMI 1640. Next, the cells were incubated with 3 μM DOX for 3 h in OPTIMEM. After washing the cover slips with PBS, they were inverted onto microscope slides; the slides were placed under the Olympus UPLFLN40× objective (NA 0.75) of an Olympus BX-50 microscope coupled with an Olympus DP71 digital color camera, used to obtain both brightfield and fluorescence microscopy images. Fluorescence excitation was facilitated with a Mercury USH 102D lamp (Ushio Inc.) while fluorescence emission was imaged with use of a DAPI/FITC/TRITC filter (Chroma Technology Corp).

Confocal Microscopy

DU145 cells were inoculated on 22 mm cover slips housed in 35 mm petri dishes (10×10^5) and left to grow overnight in 2 ml of complete RPMI 1640 in the same conditions as elaborated earlier in the "Cell Culture" section. Next, we incubated the cells with 250 nm PEI-TPP-DOX for 3 h in OPTIMEM. The mitochondrial probe mitoTracker® Green FM (200 nM) was added to cells 15 min prior to live imaging. After washing the cover slips with PBS, they were inverted onto microscope slides; the slides were placed under the ×60 oil immersion quartz objective (NA 1.3) of a Biorad MRC 1024ES laser scanning confocal microscope. Both intracellular DOX and mitoTracker® Green FM were excited using the 488 nm argon–krypton ion laser line. MitoTracker® Green FM fluorescence was collected through a band-pass filter centred at 522 (±35) nm, while DOX fluorescence was collected after a long-pass filter at ≥585 nm. Cross talk was eliminated using cell groups incubated with PEI-TPP-DOX or mitoTracker® Green FM alone. In this sense the red channel signal was purely DOX fluorescence and not MitoTracker® Green FM fluorescence "spillover" from the green channel. During image acquisition a level 3 (three iterations per image) Kalman smoothing routine was applied in all occasions to eliminate spurious signals.

Lactate Dehydrogenase (LDH) Leakage Assay

DU145 cells seeded in 35 mm petri dishes (5×10^5) were left to incubate in complete media containing 10% FBS for 24 h. The cells were subsequently incubated with 0, 100, 250, 500, 750 and 1000 nM PEI-TPP-DOX in OPTIMEM (2 mL/dish) for 3 h. Immediately following incubation, the cell media (supernatants) were removed from all cell groups and put on ice. The media-control cells, following their supernatant (100% survival control) removal, were washed with PBS, trypsinized and centrifuged. The resulting cell pellet was resuspended in 200 μL d.d. H_2O containing 5 μL Triton-X-100 10% and agitated for 30 s; The volume was supplemented with d.d. H_2O (Type II water) up to 2 mL to constitute the 100% death control.

An assay reaction mixture (pH = 7.4) was prepared containing 100 mM Tris.HCl, 0.4 mg/mL NADH and 0.1 mL/mL of 200 mM pyruvate stock. 400 μL of the mix was added to 400 μL of sample (all collected supernatants; media-control cell lysate which signified 100% death; OPTIMEM only control) in a quartz, 1 cm pathlength, 1 mL cuvette; the decay absorbance kinetics of NADH oxidation to NAD^+ through pyruvate conversion to L-lactic acid as facilitated by lactate dehydrogenase (LDH), were in each case monitored at 340 nm ($\varepsilon_{NADH\ 340nm} = 0.00622\ L\cdot\mu mol^{-1}\cdot cm^{-1}$), using a CARY 100 CONC

UV-visible spectrophotometer (Varian Inc). It has to be noted that the definition of 1 unit of LDH is the amount that will reduce 1.0 μM of pyruvate to L-Lactate per minute at pH 7.5 and 37°C. Hence we calculated LDH (U/L) = ($\Delta A\ min^{-1}/0.00622\ L\ \mu M^{-1}\ cm^{-1}$), from the slopes (ΔA/min) of the initial linear regions of the registered NADH → NAD^+ decay curves.

Lysosomal Integrity (Hexosaminidase) Assay

DU145 human prostate cancer cells were inoculated (20×10^3) into 96-well plates and left to incubate in complete media containing 10% FBS for 24 h. Cells were then treated with 0, 50,100, 250, 500, 750 and 1000 nM PEI-TPP-DOX for 3 h in OPTIMEM. At 0 and 24 h following treatment, the cells were assayed for their lysosomal hexosaminidase activity (45), relating to cell survival. All samples were incubated for 2 h in 0.05 M citric acid pH 5 containing 3.75 mM p-nitrophenyl-*N*-acetyl-β-D-glucosaminide PNNAG and 0.25% Triton X-100. Subsequently stop buffer containing 50 mM glycine and 5 mM EDTA at pH 10.4 was added to all samples. Endpoint absorbance was read in a Tecan Infinite M200 plate reader at 405 nm. Blanks containing substrate and stop buffer were subtracted from all registered values.

MTT Assay

DU145 human prostate cancer cells were inoculated (20×10^3) into 96-well plates and left to incubate in complete media containing 10% FBS for 24 h. Cells were then treated with PEI-TPP-DOX, DOX or vehicle (PEI-TPP) for 3 h in OPTIMEM. The mitochondrial redox function (translated as cell viability at $t\geq24$ h post-incubation) of all cell groups was assessed by the MTT assay at selected time points, namely immediately post-incubation (0 h) and: 24, 48, 72 h later. This was performed by replacing cell media with complete media containing 1 mg/mL MTT and incubating at 37°C in a 5% CO_2 humidified atmosphere for 2 h. MTT media were then removed from all cells and the produced formazan was solubilized with 100 μL DMSO per well. The plates were subsequently shaken for 10 min at 100 rpm in a Stuart SI500 orbital shaker, and the endpoint absorbance measurements at 562 nm were made in an Infinite M200 plate reader (Tecan group Ltd., Männedorf, Switzerland). Blank values measured in wells with DMSO and no cells, were in all cases subtracted.

Trypan Blue Assay

5×10^5 cells seeded in 35 mm petri dishes were left to incubate in complete media containing 10% FBS for 24 h. The cells were subsequently incubated with 0 (media control), 100, 250, 500 and 750 nM PEI-TPP-DOX in OPTIMEM (2 mL/dish) for 3 h. Immediately following this incubation, the cells were washed with PBS, trypsinized centrifuged and resuspended in RPMI 1640 without FBS. A 0.4% w/v PBS solution of Trypan blue was subsequently added to each cell suspension and allowed 2–3 min to stand. The cells were counted with the use of a hemocytometer to determine total and necrotic cell populations in each sample. Trypan blue is a well documented exclusion assay; cells with compromised membranes are stained blue, while cells with intact membranes are left unstained.

DNA Laddering Assessment

Cell DNA fragmentation after treatment of DU145 cells with PEI-TPP-DOX was monitored by a gel electrophoresis method, according to Eastman protocol (46). Briefly, 10^6 cells treated with 100, 300, 500 and 750 μM of PEI-TPP-DOX for 3 h were harvested at different timepoints (0.5–5 h i.e. up to 2 h post-incubation) transferred into 2% agarose gel wells, where they were lysed by a cocktail of SDS, proteinase K, and ribonuclease A. As a positive control, other cell groups were treated with 2 μM of staurosporine for 24 h which has been shown to provoke apoptotic death in DU145 cells (47). All treated cell lysates, including untreated DU145 cells as control, were subjected to electrophoresis on a 2% agarose gel. High molecular weight (HMW) DNA fragments were trapped in or near the wells, whereas lower molecular weight DNA fragments were expected to migrate to distances inversely proportional to their sizes through the gel. The gel was subsequently stained with 10% ethidium bromide, washed twice with d.d. H_2O and visualized in a UV transilluminator.

Inhibitor/Modulator Treatment of Cells

The inhibitors/modulators (primarily mitochondrial) employed, presented in Table S2 (Supplementary Material) along with their mode action and final concentrations applied, were added to the appropriate cell groups in 96 well plates 24 h following inoculation. The cells were left to incubate for 2 h and PEI-TPP-DOX (500 nM) was subsequently added to both the PEI-TPP-DOX-only and the PEI-TPP-DOX+ inhibitor cell groups in OPTIMEM for 3 h. During this time the inhibitors were maintained in the appropriate cell groups (inhibitor-only and PEI-TPP-DOX+ inhibitor). At the end of PEI-TPP-DOX incubation, OPTIMEM media were replaced with RPMI 1640 containing 10% FBS in all cell groups whilst all inhibitors were reinstated in the inhibitor-only and PEI-TPP-DOX+ inhibitor cell groups. Twenty-four hours after PEI-TPP-DOX incubation the viability was assayed in all cell groups using MTT (*vide supra*). In all cases the appropriate media-only,

PEI-TPP-DOX-only and inhibitor-only controls were included while cell media DMSO content (where applicable) was at all times kept ≤0.25%.

Statistics

All experiments were repeated independently at least three times. MTT and hexosaminidase activity data are shown as means of at least six independent values with error bars representing one standard deviation. Student paired t-tests were performed on the MTT cytotoxicity data obtained between PEI-TPP-DOX only and PEI-TPP-DOX+ inhibitor cell groups. In the related figure (Fig. 3) the statistical significance follows the assignment: ** $p<0.01$, *** $p<0.001$ and ***** $p<0.00001$ while no annotation implies no statistical significance, $p>0.05$.

RESULTS

PEI was initially characterized by inverse-gate decoupling 13C NMR. Comparing the integration of carbons adjacent to primary, secondary and tertiary amine groups, the ratio of primary to secondary to tertiary amines of PEI was calculated to be 35:38:26, as exemplified in the bibliography (48). The degree of PEI branching was found to be 0.62 and its average number of primary amine groups was determined as 10. Based on the above, the introduction of decyltriphenylphosphonium groups to PEI was attained by reacting the primary amines of PEI with (10-carboxydecyl)triphenylphosphonium bromide at a 1:2.5 M stoichiometry, using HBTU/HOBt/DIEA as coupling reagents (Scheme 1). The structure of the final product, PEI-TPP, was confirmed by ^{1}H and ^{13}C NMR spectroscopy and the degree of substitution was determined by inverse-gated decoupling ^{13}C NMR (see also Supplementary Material Figs. S1, S2). On the average, two alkylTPP groups were attached to the dendritic scaffold as determined by integration of the peaks at 36.7–40.6 ppm attributed to the α carbon of PEI relative to the newly formed amide moieties ($\underline{C}H_2NHCO$) and the α carbon relative to the remaining primary amino groups ($NH_2\underline{C}H_2$) and the peak at 35.8 ppm attributed to the α carbon of lipophilic spacer relative to the newly formed amide moieties ($NHCO\underline{C}H_2$).

PEI-TPP is water insoluble but has the ability to form colloidal dispersions in aqueous media such as PBS buffer or OPTIMEM. PEI-TPP nanoparticles as well as DOX-loaded PEI-TPP-DOX nanoparticles were prepared and subsequently the resulting nano-assemblies were characterized using dynamic light scattering (DLS) and ζ-potential. Employing a concentration of 40 μM PEI-TPP in OPTIMEM, it was possible to prepare nanoparticles with diameter of ~100 nm as revealed by DLS. Analogous sizes were obtained for DOX-loaded PEI-TPP-DOX nanoparticles. The encapsulation of DOX into PEI-TPP nanoparticles was determined by measuring the concentration of the drug in nanoparticle dispersion employing UV–vis spectroscopy after removal of the non-encapsulated DOX by ultracentrifugation. The final concentration of encapsulated DOX was consistently found to be c.a. 50 μM in a dispersion containing 40 μM PEI-TPP which corresponds to a loading capacity of 32% w/w. DOX encapsulation also affected the ζ-potential of the nanoparticles. Indeed, while the ζ-potential value of unloaded PEI-TPP nanoparticles was found to be 14±1 mV, DOX-loaded nanoparticles registered a value of 40±1 mV due to the additional positive charge conferred on the nanoparticles by doxorubicin hydrochloride [isoelectric point of DOX=8.25 (49)].

Following physicochemical characterization we proceeded with administration of PEI-TPP-DOX to DU145 cells. Our first aim was to prove that our nanocarriers effectively and specifically delivered their DOX cargo to cell mitochondria. To achieve this we employed confocal microscopy and exploited the inherent fluorescence of DOX. A representative confocal image is shown in Fig. 1. Co-localisation (yellow) of DOX (red) with the mitochondrial indicator mitotracker® green FM (green) fluorescence, shows the high specificity of our nanocarriers to cell mitochondria even at the low incubation concentration of 250 nM with respect to their DOX content. Although the nuclear affinity of free DOX is well documented, we proceeded with epi-fluorescence microscopy on DU145 cells treated with 3 μM DOX for 3 h. An indicative image, its corresponding brightfield image and their overlay appear in the bottom row of Fig. 1, showing the free DOX specificity to cell nuclei. Once the mitochondrial affinity of PEI-TPP-DOX was established, we embarked on a progressive study of its cytotoxic profile. Initially PEI-TPP (vehicle), free DOX and PEI-TPP-DOX (1, 3 and 5 μM), were administered to cells for 3 h; the viability of the cell groups was assessed at 24, 48 and 72 h post-incubation by standard MTT assays. The results summarized in Fig. 2a, show that although vehicle toxicity increased over time and concentration, it was less than 25% in all cases, while at 1 μM and assayed at 24 h it was negligible. DOX toxicity was again found to be again progressive with time and concentration and the maximum value was ~75% when assayed at 72 h and for 5 μM incubation concentration. PEI-TPP-DOX nanoparticles, however exhibited ~100% toxicity for all concentrations and all assay time points. Therefore we proceeded to a dose response study by incubating the cells with 0, 50, 100, 250, 500, 750 and 1000 nM PEI-TPP-DOX for 3 h and performed MTT assays at two time points: immediately following incubation (0 h) and 24 h post-incubation. The results shown in Fig. 2b are quite remarkable; a rapid toxicity trend, almost identical for the two time points

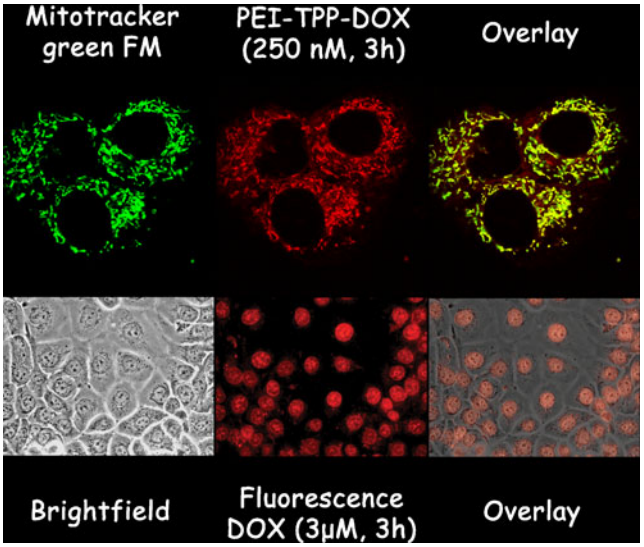

Fig. 1 PEI-TPP-DOX *vs.* DOX subcellular localization. *Top row*: Confocal fluorescence microscopy on DU145 cells incubated with 250 nM PEI-TPP-DOX for 3 h and 200 nM MitoTracker® Green FM for 15 min. *Bottom row*: Brightfield and epifluorescence microscopy on DU145 cells incubated with 3 μM free DOX for 3 h.

was obtained, with an extrapolated LD_{50} at c.a. 350 nM. Since MTT is inherently an assay of mitochondrial redox function we needed to verify the cell death, especially at 0 h; consequently we performed a lactate dehydrogenase (LDH) leakage assay at this specific end-of-incubation time point. This assay monitors the leakage of cytosolic LDH from the ruptured cytoplasmic membranes of dead cells into the surrounding culture media. The results are presented in Fig. 2c. The initial 1 min linear parts of the absorbance decay curves were each time fitted to yield the enzymic activity rates. It is evident from Fig. 2c that for DOX-equivalent concentrations ≥250 nM there was a serious LDH seepage from cell cytoplasms reaching the entire cell LDH capacity (LDH activity comparable to media control cell lysates) at DOX concentrations above 500 nM. The fitted parameters of Fig. 2c decay curves are presented in Table S1 (Supplementary Material) along with the calculated LDH activities expressed in units·L^{-1}. Furthermore, a trypan blue (TB) exclusion assay was performed immediately following 3 h cell incubation with PEI-TPP-DOX, 0–750 nM; the results shown in Fig. 2d, summarize both total and live (TB exclusive) cell counts for each PEI-TPP-DOX concentration studied. The TB data correlate very well to the 0 h MTT data (Fig. 2a), further revealing that cell death is reflected both through cell detachment and loss of membrane integrity of cells remaining attached. The latter fact is also shown by application of the lysosomal integrity—hexosaminidase assay which at 0 h shows substantial activity even at the lethal 1000 nm (Fig. 2b); therein, at 1000 nM ~60% of the hexosaminidase activity is lost (detached cells) while the registered ~40% activity is due to attached yet compromised and non-functional cells (as shown by the relevant assays), maintaining lysosomal integrity. When assayed at 24 h the hexosaminidase activity exhibited a better correlation with the corresponding MTT data. Nevertheless there was still some elevated, residual hexosaminidase activity (~15%) for cell groups incubated with 1000 nm PEI-TPP-DOX.

All the above described results delineate a rapid cell death profile even at nanomolar PEI-TPP-DOX concentrations after merely 3 h of incubation. Next we tried to assess any DNA fragmentation within the timeframe of the registered cytocide, which would link cell death to upstream apoptotic events. No DNA laddering was registered within 0.5–5 h from the start of incubation in cells treated with 100–750 nM PEI-TPP-DOX for 3 h as shown in the representative gel image (Fig. S3, Supplementary Material).

As evidenced above, DOX cytotoxicity is profoundly enhanced upon specific delivery to cell mitochondria by PEI-TPP nanoparticles, and the mode of cell demise changes from slow apoptotic (50) (free-DOX) to rapid death. In that context we applied a number of modulators of cell homeostasis (Table S2, Supplementary Material), most of which are modulators of mitochondrial functions, to cells treated with 500 nM PEI-TPP-DOX for 3 h. The results of these inhibitor pre-, co and post-treatments are shown in Fig. 3; most cases were without any notable effect on PEI-TPP-DOX cytotoxicity, however we observed profound cytoprotection upon ATR application (+35% survival) and moderate yet notable toxicity abrogation upon application of ANTI A and WORT (+10% and +15% survival respectively). Conversely in the case of MYXO application we observed an enhancement of PEI-TPP-DOX toxicity (−13% survival).

DISCUSSION

The present study is a progression of our previous work (34), where oligolysine scaffolds were functionalized with alkylTPP groups, to specifically target cell mitochondria. Herein, we used TPP functionalized poly(ethylene imine), PEI, which under appropriate conditions is able to form stable nanoparticles of ca. 100 nm radius in OPTIMEM. During their formation these nanoparticles were also able to encapsulate effectively water soluble compounds such as DOX. Repeated ultracentrifugations of the resulting nanocarriers allowed us to separate the unentrapped DOX and obtain loaded particles retaining the radii of the vehicle. Efficient encapsulation was proved by UV–vis spectroscopy which enabled us to determine the DOX concentration in solution. By employing a PEI-TPP concentration of 40 μM it was possible to attain a DOX concentration of 50 μM. The encapsulation of DOX was quite efficient since no measurable DOX release was registered for a period of 3 h at 37°C

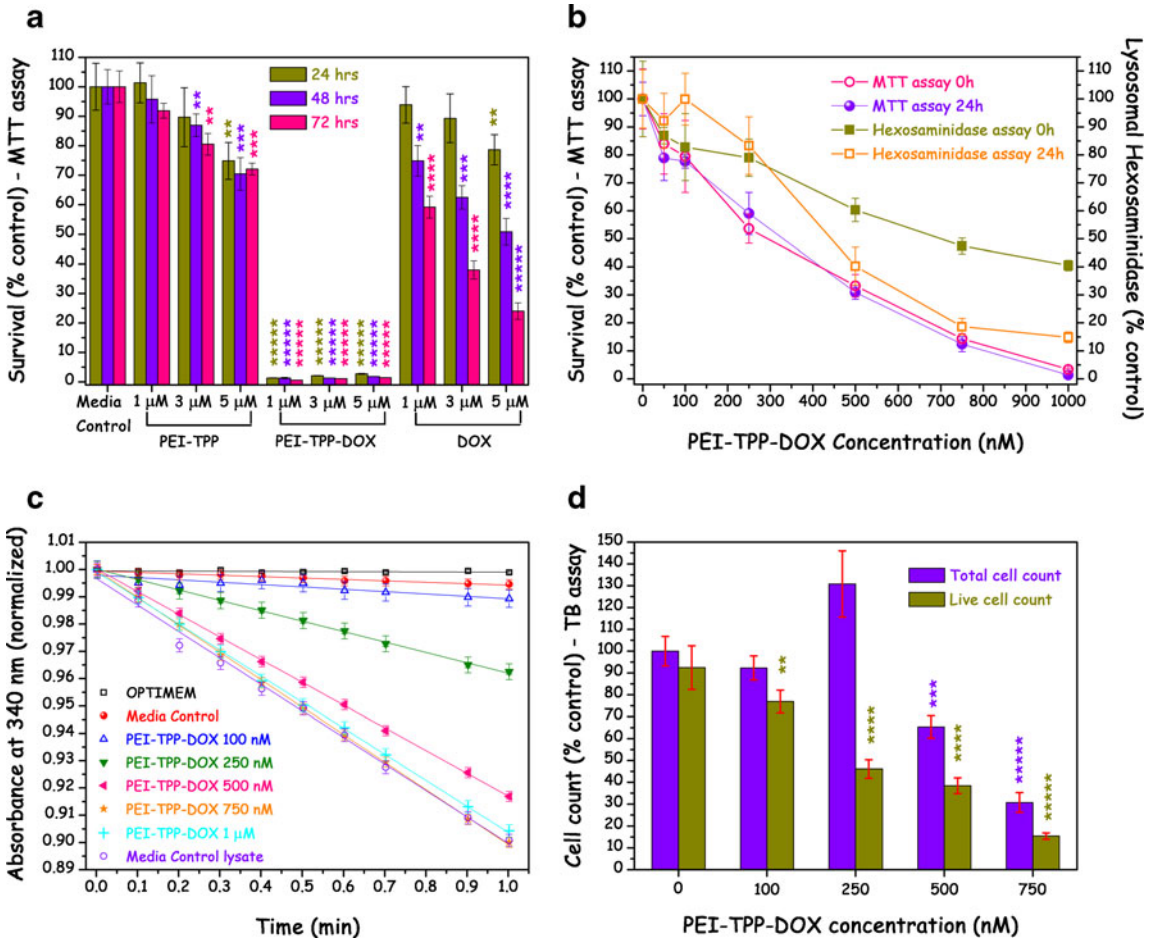

Fig. 2 PEI-TPP-DOX toxicity studies. (**a**) Comparative toxicities of PEI-TPP (vehicle), PEI-TPP-DOX and free DOX on DU145 cells following incubation at 1,3,5 μM for 3 h as revealed by MTT assays 24, 48 and 72 h following incubation. (**b**) PEI-TPP-DOX toxicity *vs* incubation (3 h) concentration as assayed by MTT and concomitant lysosomal hexosaminidase activities; both MTT and hexosaminidase assays were performed at 0 and 24 h post incubation. (**c**) LDH activity rate assays on DU145 cells incubated for 3 h with various PEI-TPP-DOX concentrations; the assays were performed immediately following incubation. (**d**) Trypan Blue exclusion assays on DU145 cells incubated for 3 h with various PEI-TPP-DOX concentrations; the assays were performed immediately following incubation. The statistical significance, as accrued by student paired t-tests follows the assignment: ** $p < 0.01$, *** $p < 0.001$, **** $p < 0.0001$ and ***** $p < 0.00001$ while no annotation implies no statistical significance, $p > 0.05$.

in OPTIMEM by fluorescence spectroscopy, i.e., within the timeframe of cell incubation with PEI-TPP-DOX throughout the *in vitro* experiments presented herein.

The microscopy studies performed on PEI-TPP-DOX loaded cells show a definite mitochondrial localization, as opposed to the predominantly nuclear pattern characteristic of free DOX but also of liposomal DOX (51); this confirms the efficient delivery to cell mitochondria with high specificity facilitated by the TPP functionalized PEI-TPP nanoparticles.

The subsequent toxicity, DNA fragmentation and functionality studies concurred to a rapid onset of a non-apoptotic death following treatment of DU145 cells with submicromolar doses of PEI-TPP-DOX; this was further reinforced by the null effects of caspase 8 and 9 inhibitors application. Administration of WORT, a well-known autophagy inhibitor (52), further indicated that part of the rapid and profound cytocide could be due to aberrant stimulation of autophagy (presumably mitophagy) which can eventually promote cell death (53). On the other hand the results of the LDH leakage assay and TB assay confirm a major component of rapid necrotic cell demise. The MTT assay summarizes the whole picture of fast, dose-dependent and lethal loss of function.

The mode of PEI-TPP-DOX associated cell death is totally different from the slow and apoptotic (50) cytotoxicity of free DOX, which even for micromolar concentrations presents a substantial residual cell survival at 72, hrs in our treatment regime. It has to be noted that the PEI-TPP vehicle was virtually non-toxic especially at 24 h and at 1000 nM concentration.

The work presented herein is, to the best of our knowledge, the first account of DOX direct action on the mitochondria of intact living cells. A few studies (54,55) had

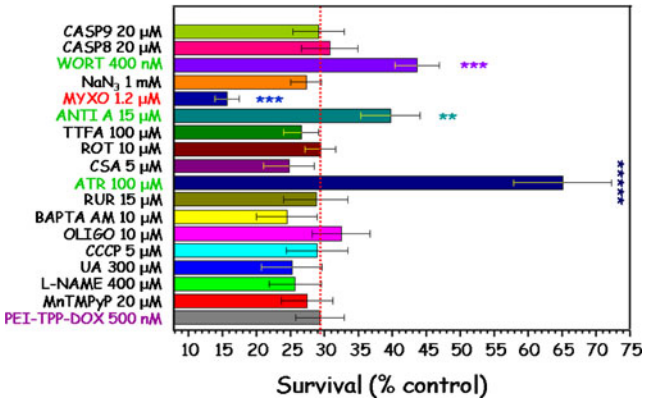

Fig. 3 DU145 cell survival rates following PEI-TPP-DOX treatment in conjunction with various modulators. The inhibitors/modulators were in all cases added to DU145 cells 2 h prior to PEI-TPP-DOX (500 nM) treatment. The cells were co-incubated with PEI-TPP-DOX and the relevant inhibitor/modulator for 3 h. After PEI-TPP-DOX incubation all modulators were maintained in the inhibitor-only and PEI-TPP-DOX+ inhibitor cell groups. Cell viability was assayed 24 h post-PEI-TPP-DOX incubation by MTT assays. The *red dashed line* denotes cell survival following incubation with PEI-TPP-DOX and no modulator. Inhibitors with cytoprotective effects appear in *green* while modulators potentiating cytotoxicity appear in *red*. The statistical significance, as accrued by student paired t-tests follows the assignment: ** $p < 0.01$, *** $p < 0.001$ and ***** $p < 0.00001$ while no annotation implies no statistical significance, $p > 0.05$.

previously addressed the direct application of DOX, nevertheless to isolated mitochondria. In their early account (54), Bachmann and Zbinden postulated that DOX caused marked inhibition of electron transfer reactions (inhibition of oxygen consumption in state III respiration) and of Ca^{2+} uptake into mitochondria. Elsewhere (55), it was shown that in the presence of ANTI A, the rate of superoxide production from isolated rat heart mitochondria was profoundly enhanced upon treatment with DOX. Moreover studies on mice treated with DOX (56), show enhanced superoxide and NO generation leading to lethal peroxynitrite ($ONOO^-$) formation. In the present study MnTMPyP, L-NAME and UA all failed to modulate the cytotoxic effect of PEI-TPP-DOX. These null effects indicate that the PEI-TPP-DOX associated cell death is most probably not related to superoxide anion and/or related ROS (e.g. concomitant H_2O_2 following dismutation), NO, or superoxide-NO related pathways (e.g. concomitant formation of deleterious $ONOO^-$).

The application of ATR, yielded a profound abrogation of PEI-TPP-DOX associated cytotoxicity. This cytoprotection however cannot be assigned to inhibition of ATP and ADP transport through the adenine nucleotide translocator (57) (ANT), given the null effects of both OLIGO and CCCP which indicate no dependence of the PEI-TPP-DOX toxicity to ATP production and hence availability. However, in addition to its main function, the ANT also forms the inner membrane channel of the mitochondrial permeability transition pore (MPTP); ATR binding promotes channel formation (58), which is enhanced in the presence of BAX (58,59) possibly causing permanent MPTP opening. Transient, asynchronous channel openings however in the absence of BAX (58), as in our case of BAX-deficient DU145 (60), have been found to be protective through alleviation of mitochondrial Ca^{2+} overload (61). In the present circumstances, the use of CSA excluded the involvement of MPTP in the PEI-TPP-DOX cytotoxicity; the null results of intracellular Ca^{2+} chelator BAPTA AM and mitochondrial Ca^{2+} uniporter inhibitor RUR, further preclude any involvement of Ca^{2+} mobility. ATR-related transient channel formation could nevertheless facilitate a direct DOX effluence from the mitochondria. In retrospect, this later prospect could also apply to previously encountered instances of ATR protective action (62,63), regarding agents other than PEI-TPP-DOX.

A moderate cytoprotective action was also effected by ANTI A; this inhibitor of mitochondrial electron transport chain (ETC) complex III quinone reducing centre (q_i), most probably blocked the deleterious effects of DOX semiquinone radical (64,65), which can be preferentially generated at q_i, due to the enhanced stability of semiquinones at that site (66), by one-electron donation. In contrast application of MYXO, exacerbated the PEI-TPP-DOX associated cell toxicity, possibly (reversing the ANTI A logic) due to inhibition of DOX semiquinone radical re-reduction to DOX at the quinoloxidising centre (q_o) of ETC complex III. Complex III is well documented as a site of electron leakage in the ETC, resulting in the formation of superoxide and H_2O_2 (67,68) while the combination of DOX and ANTI A in intact mitochondria was previously found to profoundly enhance this ROS production (55). The herein observed protective effect of ANTI A together with the null effects of MnTmPyP, UA and L-NAME (*vide supra*) further confirm that the severe cytotoxicity conferred by PEI-TPP-DOX cannot not be primarily ascribed to superoxide anion, (and concomitant H_2O_2 or $ONOO^-$), otherwise application of ANTI A would have further potentiated the cytocide. The effects of ATR, ANT1, MYXO and WORT are summarized in Table S3 (Supplementary Material).

In the present study, apart for developing very efficient dendrimer-based mitotropic nanoparticles, we also demonstrated the severe cytocidal effects of DOX applied to live cell mitochondria. The fact that PEI-TPP-DOX induces an acute necrotic stimulus has certain advantages, such as the potential for inflammatory response activation; in contrast to apoptosis where cells die "quietly", necrosis may act as a "loud" immune distress signal (69). In cells undergoing necrotic assault, along with the majority of the intracellular content effluence from the compromised plasma membranes, several cytosolic molecules associated with necrosis-induced immune signalling also escape by passive diffusion (69). With regard to PEI-TPP-DOX, an indication in support of this eventuality is the fact that some cells, although lethally compromised (TB, MTT)

remained attached—even retained lysosomal integrity (hexosaminidase activity)—while they "spewed out" their cytosolic contents (e.g. LDH).

Given the fact that nowadays necrosis is no longer considered to be an uncontrolled or pathological yet rapid mode of cell death, but is in contrast widely regarded to be analogous to an active or programmed form of cell death, cancer biologists have started to consider whether efficient anticancer agents might instigate necrotic cell death (69).

Albeit, PEI-TPP-DOX nanoparticles could be appropriately functionalized to actively target cancer cells in future work, even in their present form they are expected to exhibit passive targeting, through the enhanced permeability and retention (EPR) effect (70,71). EPR is a result of the leaky vascular endothelial linings of growing neoplasias, leaving gaps in the endothelium of up to 800 nm in diameter, large enough to permit the extravasation of nanocarriers (e.g. liposomes) with diameters in the range of 100–200 nm (72). Moreover, the defective lymphatic drainage of developing tumors, extends the residence time of extravasated nanocarriers in the tumor extracellular space; this could allow PEI-TPP-DOX to efficiently and selectively target tumor cell mitochondria *in vivo* which remains to be seen in future work.

REFERENCES

1. Duchen MR. Mitochondria in health and disease: perspectives on a new mitochondrial biology. Mol Aspects Med. 2004;25(4):365–451.
2. Zhang DX, Gutterman DD. Mitochondrial reactive oxygen species-mediated signaling in endothelial cells. Am J Physiol Heart Circ Physiol. 2007;292(5):H2023–31.
3. Murphy MP. How mitochondria produce reactive oxygen species. Biochem J. 2009;417(1):1–13.
4. Oberst A, Bender C, Green DR. Living with death: the evolution of the mitochondrial pathway of apoptosis in animals. Cell Death Differ. 2008;15(7):1139–46.
5. DiMauro S. Mitochondrial diseases. Biochim Biophys Acta. 2004;1658(1–2):80–8.
6. Reardon W, Ross RJ, Sweeney MG, Luxon LM, Pembrey ME, Harding AE, *et al.* Diabetes mellitus associated with a pathogenic point mutation in mitochondrial DNA. Lancet. 1992;340(8832):1376–9.
7. Carew JS, Huang P. Mitochondrial defects in cancer. Mol Cancer. 2002;1:9.
8. Adlam VJ, Harrison JC, Porteous CM, James AM, Smith RA, Murphy MP, *et al.* Targeting an antioxidant to mitochondria decreases cardiac ischemia-reperfusion injury. FASEB J. 2005;19(9):1088–95.
9. Weissig V. Mitochondrial delivery of biologically active molecules. Pharm Res. 2011;28(11):2633–8.
10. Weissig V. From serendipity to mitochondria-targeted nanocarriers. Pharm Res. 2011;28(11):2657–68.
11. Del Gaizo V, Payne RM. A novel TAT-mitochondrial signal sequence fusion protein is processed, stays in mitochondria, and crosses the placenta. Mol Ther. 2003;7(6):720–30.
12. Horton KL, Stewart KM, Fonseca SB, Guo Q, Kelley SO. Mitochondria-penetrating peptides. Chem Biol. 2008;15(4):375–82.
13. Kelley SO, Stewart KM, Mourtada R. Development of novel peptides for mitochondrial drug delivery: amino acids featuring delocalized lipophilic cations. Pharm Res. 2011;28(11):2808–19.
14. Geisler IM, Chmielewski J. Dimeric cationic amphiphilic polyproline helices for mitochondrial targeting. Pharm Res. 2011;28(11):2797–807.
15. Cocheme HM, Kelso GF, James AM, Ross MF, Trnka J, Mahendiran T, *et al.* Mitochondrial targeting of quinones: therapeutic implications. Mitochondrion. 2007;7(Suppl):S94–102.
16. Dessolin J, Schuler M, Quinart A, De Giorgi F, Ghosez L, Ichas F. Selective targeting of synthetic antioxidants to mitochondria: towards a mitochondrial medicine for neurodegenerative diseases? Eur J Pharmacol. 2002;447(2–3):155–61.
17. Smith RA, Kelso GF, James AM, Murphy MP. Targeting coenzyme Q derivatives to mitochondria. Methods Enzymol. 2004;382:45–67.
18. Tauskela JS. MitoQ—a mitochondria-targeted antioxidant. IDrugs. 2007;10(6):399–412.
19. Murphy MP, Smith RA. Targeting antioxidants to mitochondria by conjugation to lipophilic cations. Annu Rev Pharmacol Toxicol. 2007;47:629–56.
20. Lei W, Xie J, Hou Y, Jiang G, Zhang H, Wang P, *et al.* Mitochondria-targeting properties and photodynamic activities of porphyrin derivatives bearing cationic pendant. J Photochem Photobiol B. 2010;98(2):167–71.
21. Fernandez-Carneado J, Van Gool M, Martos V, Castel S, Prados P, de Mendoza J, *et al.* Highly efficient, nonpeptidic oligoguanidinium vectors that selectively internalize into mitochondria. J Am Chem Soc. 2005;127(3):869–74.
22. Sibrian-Vazquez M, Nesterova IV, Jensen TJ, Vicente MG. Mitochondria targeting by guanidine- and biguanidine-porphyrin photosensitizers. Bioconjug Chem. 2008;19(3):705–13.
23. Armstrong JS. Mitochondrial medicine: pharmacological targeting of mitochondria in disease. Br J Pharmacol. 2007;151(8):1154–65.
24. Cuchelkar V, Kopeckova P, Kopecek J. Novel HPMA copolymer-bound constructs for combined tumor and mitochondrial targeting. Mol Pharm. 2008;5(5):776–86.
25. Horobin RW, Trapp S, Weissig V. Mitochondriotropics: a review of their mode of action, and their applications for drug and DNA delivery to mammalian mitochondria. J Control Release. 2007;121(3):125–36.
26. Mukhopadhyay A, Weiner H. Delivery of drugs and macromolecules to mitochondria. Adv Drug Deliv Rev. 2007;59(8):729–38.
27. Weissig V, Cheng SM, D'Souza GG. Mitochondrial pharmaceutics. Mitochondrion. 2004;3(4):229–44.
28. Yamada Y, Harashima H. Mitochondrial drug delivery systems for macromolecule and their therapeutic application to mitochondrial diseases. Adv Drug Deliv Rev. 2008;60(13–14):1439–62.
29. Duchen MR. Roles of mitochondria in health and disease. Diabetes. 2004;53 Suppl 1:S96–102.
30. Biswas S, Dodwadkar NS, Piroyan A, Torchilin VP. Surface conjugation of triphenylphosphonium to target poly(amidoamine) dendrimers to mitochondria. Biomaterials. 2012;33(18):4773–82.
31. Biswas S, Dodwadkar NS, Sawant RR, Koshkaryev A, Torchilin VP. Surface modification of liposomes with rhodamine-123-conjugated polymer results in enhanced mitochondrial targeting. J Drug Target. 2011;19(7):552–61.
32. Samuelson LE, Dukes MJ, Hunt CR, Casey JD, Bornhop DJ. TSPO targeted dendrimer imaging agent: synthesis, characterization, and cellular internalization. Bioconjug Chem. 2009;20(11):2082–9.
33. Zhang L, Yao HJ, Yu Y, Zhang Y, Li RJ, Ju RJ, *et al.* Mitochondrial targeting liposomes incorporating daunorubicin and quinacrine for treatment of relapsed breast cancer arising from cancer stem cells. Biomaterials. 2012;33(2):565–82.

34. Theodossiou TA, Sideratou Z, Tsiourvas D, Paleos CM. A novel mitotropic oligolysine nanocarrier: targeted delivery of covalently bound D-Luciferin to cell mitochondria. Mitochondrion. 2011;11(6):982–6.
35. Boddapati SV, D'Souza GG, Erdogan S, Torchilin VP, Weissig V. Organelle-targeted nanocarriers: specific delivery of liposomal ceramide to mitochondria enhances its cytotoxicity in vitro and in vivo. Nano Lett. 2008;8(8):2559–63.
36. Huang K, Voss B, Kumar D, Hamm HE, Harth E. Dendritic molecular transporters provide control of delivery to intracellular compartments. Bioconjug Chem. 2007;18(2):403–9.
37. Lim CS. Organelle-specific targeting in drug delivery and design. Adv Drug Deliv Rev. 2007;59:697.
38. Boddapati SV, Tongcharoensirikul P, Hanson RN, D'Souza GG, Torchilin VP, Weissig V. Mitochondriotropic liposomes. J Liposome Res. 2005;15(1–2):49–58.
39. Weissig V, Boddapati SV, Cheng SM, D'Souza GG. Liposomes and liposome-like vesicles for drug and DNA delivery to mitochondria. J Liposome Res. 2006;16(3):249–64.
40. Malhi SS, Budhiraja A, Arora S, Chaudhari KR, Nepali K, Kumar R, *et al.* Intracellular delivery of redox cycler-doxorubicin to the mitochondria of cancer cell by folate receptor targeted mitocancerotropic liposomes. Int J Pharm. 2012;432(1–2):63–74.
41. Mo R, Sun Q, Xue J, Li N, Li W, Zhang C, *et al.* Multistage pH-responsive liposomes for mitochondrial-targeted anticancer drug delivery. Adv Mater. 2012;24(27):3659–65.
42. Marrache S, Dhar S. Engineering of blended nanoparticle platform for delivery of mitochondria-acting therapeutics. Proc Natl Acad Sci U S A. 2012;109(40):16288–93.
43. Sharma A, Soliman GM, Al-Hajaj N, Sharma R, Maysinger D, Kakkar A. Design and evaluation of multifunctional nanocarriers for selective delivery of coenzyme Q10 to mitochondria. Biomacromolecules. 2012;13(1):239–52.
44. Gewirtz DA. A critical evaluation of the mechanisms of action proposed for the antitumor effects of the anthracycline antibiotics adriamycin and daunorubicin. Biochem Pharmacol. 1999;57(7):727–41.
45. Landegren U. Measurement of cell numbers by means of the endogenous enzyme hexosaminidase. Applications to detection of lymphokines and cell surface antigens. J Immunol Methods. 1984;67(2):379–88.
46. Eastman A, Barry MA. Interaction of trans-diamminedichloroplatinum(II) with DNA: formation of monofunctional adducts and their reaction with glutathione. Biochemistry. 1987;26(12):3303–7.
47. Zhang H, Hoang T, Saeed B, Ng SC. Induction of apoptosis in prostatic tumor cell line DU145 by staurosporine, a potent inhibitor of protein kinases. Prostate. 1996;29(2):69–76.
48. Cao X, Li Z, Song X, Cui X, Cao P, Liu H, *et al.* Core-shell type multiarm star poly(ε-caprolactone) with high molecular weight hyperbranched polyethylenimine as core: synthesis, characterization and encapsulation properties. Eur Polym J. 2008;44:1060–70.
49. Choucair A, Soo PL, Eisenberg A. Active loading and tunable release of doxorubicin from block copolymer vesicles. Langmuir. 2005;21(20):9308–13.
50. Patel D, Chaudhary J. Increased expression of bHLH transcription factor E2A (TCF3) in prostate cancer promotes proliferation and confers resistance to doxorubicin induced apoptosis. Biochem Biophys Res Commun. 2012;422(1):146–51.
51. Theodossiou TA, Galanou MC, Paleos CM. Novel amiodarone-doxorubicin cocktail liposomes enhance doxorubicin retention and cytotoxicity in DU145 human prostate carcinoma cells. J Med Chem. 2008;51(19):6067–74.
52. Wu YT, Tan HL, Shui G, Bauvy C, Huang Q, Wenk MR, *et al.* Dual role of 3-methyladenine in modulation of autophagy via different temporal patterns of inhibition on class I and III phosphoinositide 3-kinase. J Biol Chem. 2010;285(14):10850–61.
53. Levine B, Kroemer G. Autophagy in the pathogenesis of disease. Cell. 2008;132(1):27–42.
54. Bachmann E, Zbinden G. Effect of doxorubicin and rubidazone on respiratory function and Ca^{+2} transport in rat heart mitochondria. Toxicol Lett. 1979;3:29–34.
55. Sviryaeva IV, Ruuge EK, Shumaev KB. Effect of adriamycin on superoxide radical generation in isolated heart mitochondria. Biophysics. 2007;52(6):582–6.
56. Mukhopadhyay P, Rajesh M, Batkai S, Kashiwaya Y, Hasko G, Liaudet L, *et al.* Role of superoxide, nitric oxide, and peroxynitrite in doxorubicin-induced cell death in vivo and in vitro. Am J Physiol Heart Circ Physiol. 2009;296(5):H1466–83.
57. Fiore C, Tezeguet V, LeSaux A, Roux P, Schwimmer C, Dianoux AC, *et al.* The mitochondrial ADP/ATP carrier: structural, physiological and pathological aspects. Biochimie. 1998;80:137–50.
58. Vieira HL, Haouzi D, El Hamel C, Jacotot E, Belzacq AS, Brenner C, *et al.* Permeabilization of the mitochondrial inner membrane during apoptosis: impact of the adenine nucleotide translocator. Cell Death Differ. 2000;7(12):1146–54.
59. Brenner C, Cadiou H, Vieira HL, Zamzami N, Marzo I, Xie Z, *et al.* Bcl-2 and Bax regulate the channel activity of the mitochondrial adenine nucleotide translocator. Oncogene. 2000;19(3):329–36.
60. Tang DG, Li L, Chopra DP, Porter AT. Extended survivability of prostate cancer cells in the absence of trophic factors: increased proliferation, evasion of apoptosis, and the role of apoptosis proteins. Cancer Res. 1998;58(15):3466–79.
61. Korge P, Yang L, Yang JH, Wang Y, Qu Z, Weiss JN. Protective role of transient pore openings in calcium handling by cardiac mitochondria. J Biol Chem. 2011;286(40):34851–7.
62. Theodossiou TA, Papakyriakou A, Hothersall JS. Molecular modeling and experimental evidence for hypericin as a substrate for mitochondrial complex III; mitochondrial photodamage as demonstrated using specific inhibitors. Free Radic Biol Med. 2008;45(11):1581–90.
63. Theodossiou TA, Yannakopoulou K, Aggelidou C, Hothersall JS. Tamoxifen subcellular localization; observation of cell-specific cytotoxicity enhancement by inhibition of mitochondrial ETC complexes I and III. Photochem Photobiol. 2012;88(4):1016–22.
64. Minotti G. Reactions of adriamycin with microsomal iron and lipids. Free Radic Res Commun. 1989;7(3–6):143–8.
65. Winterbourn CC, Gutteridge JM, Halliwell B. Doxorubicin-dependent lipid peroxidation at low partial pressures of O2. J Free Radic Biol Med. 1985;1(1):43–9.
66. Osyczka A, Moser CC, Dutton PL. Fixing the Q cycle. Trends Biochem Sci. 2005;30(4):176–82.
67. Andreyev AY, Kushnareva YE, Starkov AA. Mitochondrial metabolism of reactive oxygen species. Biochemistry (Mosc). 2005;70(2):200–14.
68. Chen Q, Vazquez EJ, Moghaddas S, Hoppel CL, Lesnefsky EJ. Production of reactive oxygen species by mitochondria: central role of complex III. J Biol Chem. 2003;278(38):36027–31.
69. Zong WX, Thompson CB. Necrotic death as a cell fate. Genes Dev. 2006;20(1):1–15.
70. Maeda H, Wu J, Sawa T, Matsumura Y, Hori K. Tumor vascular permeability and the EPR effect in macromolecular therapeutics: a review. J Control Release. 2000;65(1–2):271–84.
71. Maeda H, Sawa T, Konno T. Mechanism of tumor-targeted delivery of macromolecular drugs, including the EPR effect in solid tumor and clinical overview of the prototype polymeric drug SMANCS. J Control Release. 2001;74(1–3):47–61.
72. Ishida O, Maruyama K, Sasaki K, Iwatsuru M. Size-dependent extravasation and interstitial localization of polyethyleneglycol liposomes in solid tumor-bearing mice. Int J Pharm. 1999;190(1):49–56.